International Journal of Heat and Mass Transfer 55 (2012) 8051–8060

Contents lists available at SciVerse ScienceDirect

International Journal of Heat and Mass Transfer

journal homepage: www.elsevier.com/locate/ijhmt

Comparative studies on accuracy and convergence rate between the cell-centered scheme and the cell-vertex scheme for triangular grids

Guojun Yu [a], Bo Yu [a,*], Yu Zhao [a], Jinjia Wei [b]

[a] Beijing Key Laboratory of Urban Oil and Gas Distribution Technology, China University of Petroleum, Beijing 102249, People's Republic of China
[b] State Key Laboratory of Multiphase Flow in Power Engineering, Xi'an Jiaotong University, Xi'an 710049, People's Republic of China

ARTICLE INFO

Article history:
Received 5 July 2011
Received in revised form 28 April 2012
Accepted 18 August 2012
Available online 18 September 2012

Keywords:
Triangular grid
Cell-centered scheme
Cell-vertex scheme
Accuracy
Convergence rate

ABSTRACT

The truncation errors of the cell-centered and the cell-vertex schemes for unstructured triangular grids are theoretically derived respectively, showing that the truncation error of the cell-vertex scheme is smaller than that of the cell-centered scheme for the same triangular grids. The theoretical derivation is validated by some numerical examples. In addition, it is also shown by both of theoretical analysis and numerical examples that the convergence rate of the cell-vertex scheme is faster than that of the cell-centered scheme.

1. Introduction

Since 1980s, the application of unstructured triangular grids has excited our great interest because of its good adaptability to complex geometries and flexibility of local refinement. Some grid generation techniques have been presented, such as Advancing Front Technique (AFT) [1,2], Delaunay triangulation algorithm [3,4] and the Bubble Packing Method (BPM) [5,6]. Among these methods, AFT and Delaunay triangulation algorithm are widely used, while AFT and BPM can generate higher-quality unstructured grids. In addition, BPM can generate high-quality unstructured grids automatically for dynamic meshing and can be easily extended to three dimensions, and has been developed rapidly in recent years.

Similar to structured grids, there are two basic finite-volume techniques for the discretization of governing equations on unstructured grids. One is the cell-centered scheme (named Practice B in literature [7,8]), and another is the cell-vertex scheme (named Practice A in literature [8]). For the former scheme, the variables are located at the centroids of the control volumes (see Fig. 1), while for the latter, the variables are located at the vertexes. For unstructured triangular grids, there are two approaches to structure the control volumes for the cell-vertex scheme. The first approach is to connect the successive centroids of the triangular elements which share the same vertex by straight lines, thus the vertex is the node of the control volume, as shown in Fig. 2a. The second approach which is proposed by Winslow in 1967 and often applied in FEM is to join the centroids of each triangle sharing the same vertex to the midpoints of the sides of that triangle, as shown in Fig. 2b. However, the second approach is seldom employed in FVM because it is not convenient for structuring the control volumes and the numbers of neighboring elements for different control volumes are varying, thus is difficult for computation. The first approach (Fig. 2a) is employed in this article.

For the cell-centered scheme for triangular grids, the program implementation is easier because the grid cells themselves are the control volumes, and the numbers of neighboring elements of different control volumes are fixed. On the contrary, the program implementation with a cell-vertex scheme is more complex because the control volumes are not the mesh cells and thus we have to construct the control volumes separately, besides the numbers of neighboring elements for different control volumes are varying. Therefore, the cell-vertex scheme is not so popular in FVM. However, every coin has two sides, and in this article we intend to explore whether the cell-vertex scheme has some advantages in accuracy and convergence rate. As literature [9] indicated the discretization error of the cell-vertex scheme is smaller than that of the cell-centered scheme for one dimensional non-uniform grid, yet these two schemes based on quadrilateral grids give almost identical results in the calculation of a two-dimensional fluid flow problem. However, the differences in accuracy and convergence rate between these two schemes for triangular grids have not been discussed before and still need to be studied.

* Corresponding author at: Beijing Key Laboratory of Urban Oil and Gas Distribution Technology, China University of Petroleum, Beijing 102249, People's Republic of China. Tel.: +86 1089733849.
E-mail address: yubobox@vip.163.com (B. Yu).

0017-9310/$ - see front matter © 2012 Elsevier Ltd. All rights reserved.
http://dx.doi.org/10.1016/j.ijheatmasstransfer.2012.08.042

Nomenclature

a	distance between two adjacent nodes
a_H	length of the sides of hexagons
a_T	length of the sides of triangles
A	area of a face of a control volume
$\boldsymbol{A}$	face vector($=\vec{n}A$)
b	length of a face of a control volume
$\boldsymbol{d_j}$	nodal distance vector from node P_0 to P_j
D_j^c	cross derivative term
D_j^n	normal term
F_j	mass flux at surface j
g_{P_0}	weight coefficient
$\boldsymbol{n}_j$	outward unit normal vector of surface j of a control volume
S_ϕ	source term
$\boldsymbol{U}$	velocity vector
V_{P_0}	the control volume of node P_0
x_j	direction from P_0 to P_j

Greek symbols

Γ_ϕ	general diffusion coefficient
$\nabla\phi_{P_0}$	variable gradient at node P_0
$\nabla\phi_{P_j}$	variable gradient at node P_j
ξ_c	coefficient of truncation term of cell-centered scheme
ξ_v	coefficient of truncation term of cell-vertex scheme
ρ	density of fluid
ϕ	a general variable
ϕ_i	numerical solution at node i
$\hat{\phi}_i$	benchmark solution at node i
ϕ_j	variable at surface j

Subscripts

T, H	T = triangle, H = hexagon
c, v	c = center, v = vertex

For quadrilateral grids, there are no significant differences between a cell-vertex scheme and a cell-centered scheme, because the shapes and the numbers of the control volumes for the two schemes are the same. But for triangular grids, the shapes and the number of the control volumes for these two schemes are both different, e.g. for a cell-centered scheme, the control volumes are triangles while they are hexagons or polygons for a cell-vertex scheme, and the number of control volumes for a cell-centered scheme is larger than that for a cell vertex scheme. So there maybe some differences in accuracy and convergence rates between these two schemes, which is our concern in this article.

The application of unstructured triangular grids in fluid flow and heat transfer problems has a limitation that high-order schemes which are mature on structured grids are difficult to implement. When Navier–Stokes equation is discretized on triangular grids, the general schemes of convection term are FUD (First-order Upwind Difference) [10,11], SUD (Second-order Upwind Difference) [12] and CD (Central Difference). FUD has serious numerical dissipation thus is seldom used. Although CD indicates numerical instability, it is often used [13–15] on unstructured meshes if stability conditions are satisfied.

In this article, Navier–Stokes equation is discretized by the finite-volume method based on non-staggered [11,16–18] unstructured triangular grids. The convection term is discretized by deferred-correction CD and SUD scheme respectively, and the diffusion term is discretized by CD scheme. Coupling between pressure and velocity is solved by SIMPLE algorithm [10,11,19,20] based on non-staggered grid, and the velocity at the surface is calculated by pressure-weighted interpolation method [21,22].

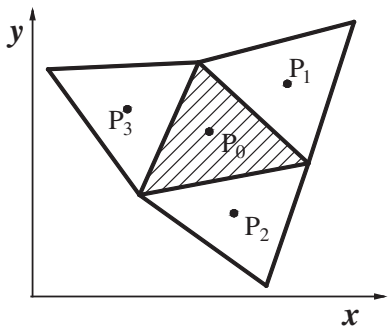

Fig. 1. Control volumes of the cell-centered scheme for the triangular grid.

2. Governing equation and discretization

The general form of the governing equation for a convection-diffusion problem can be written as follows:

$$\frac{\partial(\rho\phi)}{\partial t}+\nabla\cdot(\rho\boldsymbol{U}\phi)=\nabla\cdot(\Gamma_\phi\nabla\phi)+S_\phi, \tag{1}$$

where ϕ represents a general variable, $\boldsymbol{U}$ is a velocity vector. ρ, Γ_ϕ and S_ϕ are the density of the fluid, the general diffusion coefficient and the source term respectively. For a steady flow, Eq. (1) is reduced to

$$\nabla\cdot(\rho\boldsymbol{U}\phi)=\nabla\cdot(\Gamma_\phi\nabla\phi)+S_\phi. \tag{2}$$

Integrating general Eq. (2) over an arbitrary control volume gives

$$\int_V\nabla\cdot(\rho\boldsymbol{U}\phi)dV=\int_V\nabla\cdot(\Gamma_\phi\nabla\phi)dV+\int_V S_\phi dV. \tag{3}$$

Applying Gauss Theorem, we obtain

$$\int_A(\rho\boldsymbol{U}\phi-\Gamma_\phi\nabla\phi)\cdot d\boldsymbol{A}=\int_V S_\phi dV. \tag{4}$$

where A is the area of a face of a control volume, and $\boldsymbol{A}$ is a face vector($=\vec{n}A$).

For an N-polygonal control volume, we obtain

$$\sum_{j=1}^{N}\int_{A_j}(\rho\boldsymbol{U}\phi-\Gamma_\phi\nabla\phi)\cdot d\boldsymbol{A}=\int_{V_{P_0}}S_\phi dV. \tag{5}$$

The convection term in Eq. (5) can be discretized as

$$C_j=\int_{A_j}(\rho\boldsymbol{U}\phi)\cdot dA=(\rho\boldsymbol{U}\phi)_j\cdot\boldsymbol{A_j}=F_j\phi_j, \tag{6}$$

here ϕ_j can be calculated by the central difference scheme with a linear interpolation, i.e. $\phi_j=g_{P_0}\phi_{P_0}+(1-g_{P_0})\phi_{P_j}$, or the second-order upwind scheme [12], i.e. $\phi_j=\begin{cases}\phi_{P_0}+\nabla\phi_{P_0}\cdot(r_j-r_{P_0}) & v_n\geqslant 0\\ \phi_{P_j}+\nabla\phi_{P_j}\cdot(r_j-r_{P_j}) & v_n<0\end{cases}$, where g_{P_0} is a weight coefficient, P_0 and P_j are two adjacent nodes, F_j is mass flux at surface j, $\nabla\phi_{P_0}$ and $\nabla\phi_{P_j}$ are the variable gradient at node P_0 and P_j.The diffusion term in Eq. (5) can be discretized as

$$D_j=-\int_{A_j}\Gamma_\phi\nabla\phi\cdot d\boldsymbol{A}=-\Gamma_{\phi_j}\nabla\phi_j\cdot\boldsymbol{A_j}, \tag{7}$$

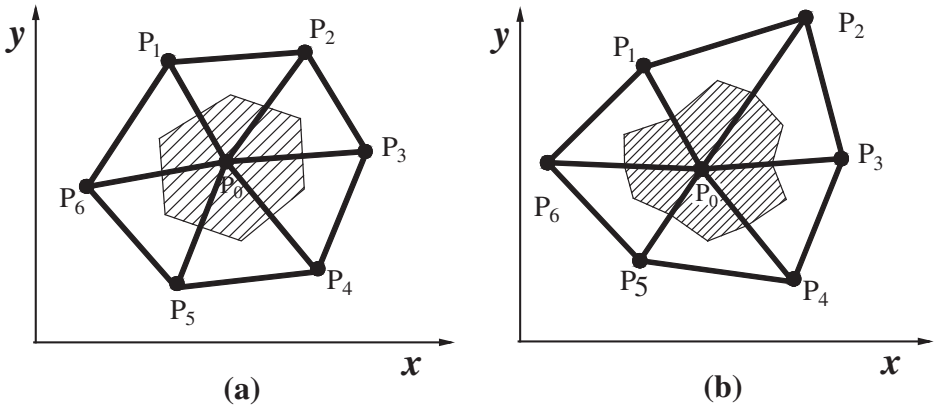

Fig. 2. Two kinds of control volumes of the cell-vertex scheme for the triangular grid.

where D_j can be divided into two terms [23] at the surface as follows:

$$D_j = D_j^n + D_j^c, \tag{8}$$

$$D_j^n = \Gamma_{\phi_j}\left(\frac{\phi_{P_j}-\phi_{P_0}}{|\boldsymbol{d_j}|}\frac{\boldsymbol{d_j}}{|\boldsymbol{d_j}|}\right)\cdot\boldsymbol{A_j}, \tag{9}$$

$$D_j^c = \Gamma_{\phi_j}\left((\nabla\phi)_j-(\nabla\phi)_j\cdot\frac{\boldsymbol{d_j}}{|\boldsymbol{d_j}|}\frac{\boldsymbol{d_j}}{|\boldsymbol{d_j}|}\right)\cdot\boldsymbol{A_j}. \tag{10}$$

In Eqs. (8)–(10), $\boldsymbol{A_j}$ is the face vector of face j, $\boldsymbol{d_j}$ is the nodal distance vector from node P_0 to P_j, D_j^c and D_j^n are the cross derivative term and the normal term respectively.The source term can be discretized as

$$\int_{V_{P_0}} S_\phi dV = S_{\phi_{P_0}} V_{P_0}. \tag{11}$$

Substituting Eqs. (6), (7), and (11) into Eq. (5) we obtain the equation in the form as below

$$a_0\phi_{P_0} = \sum_{j=1}^{N} a_j\phi_{P_j} + b_0, \tag{12}$$

where

$$a_j = \frac{\Gamma_{\phi_j}}{|\boldsymbol{d_j}|^2}(\boldsymbol{d_j}\cdot\boldsymbol{A_j}) + (\max(F_j,0)-F_j), \tag{13}$$

$$a_0 = \sum_{j=1}^{N} a_j, \tag{14}$$

$$b_0 = \sum_{j=1}^{N}\left[\Gamma_{\phi_j}\left((\nabla\phi)_j-(\nabla\phi)_j\cdot\frac{\boldsymbol{d_j}}{|\boldsymbol{d_j}|}\frac{\boldsymbol{d_j}}{|\boldsymbol{d_j}|}\right)\cdot\boldsymbol{A_j} - (\phi_j-\phi_{P_0})\max(F_j,0) + (\phi_j-\phi_{P_j})\max(-F_j,0)\right] + S_{\phi_{P_0}}V_{P_0}. \tag{15}$$

Then variable ϕ in Eq. (12) can be solved with a suitable non-linear equation solver.

3. Error analysis

The solution error will be influenced by truncation error caused by discretiztion, round-off error caused by limited characters of the computer, the error caused by incomplete iteration, and the quality of the grids. Thus it is difficult to analyze the solution error quantitatively with all these factors considered. In this article, we just concern about the difference in accuracy between the cell-centered scheme and the cell-vertex scheme, so the influences of other factors should be eliminated. For the same computer, the difference in round-off error can be ignored. And the influence of error caused by incomplete iteration could be equated. In addition, if the triangular cells are equilateral, the quality of different grids could be considered the same. So the comparison of solution errors between the cell-centered scheme and the cell-vertex scheme can be performed on equilateral grids. It is reported in [24,25] that the influences of nonorthogonality on accuracy are very slight if the mesh is not very skew. Then, we may borrow this conclusion to our case and assume if the grids do not deviate from equilateral grids severely, the conclusion obtained from equilateral grids remains. As an indicator of solution error, the truncation errors of the cell-centered scheme and the cell-vertex scheme are compared in this part.

Applying Eq. (5) and (11) to any equilateral N-polygonal control volumes in the two dimensional Cartesian coordinate, we obtain

$$\frac{\sum_{j=1}^{N}(\rho\boldsymbol{U}\phi)_j\cdot\boldsymbol{A_j}}{V_{P_0}} - \frac{\sum_{j=1}^{N}\Gamma_{\phi_j}\nabla\phi_j\cdot\boldsymbol{A_j}}{V_{P_0}} = S_{\phi_{P_0}}. \tag{16}$$

We define a as the distance between two adjacent nodes (grid size), and b as the length of a face of a control volume. For an N-polygonal control volume, Eq. (16) can be written as

$$\sum_{j=1}^{N}\rho_j\boldsymbol{U}_j\cdot\boldsymbol{n}_j\phi_j\frac{b}{\Delta V} - \sum_{j=1}^{N}\Gamma_j\frac{\frac{\phi_{P_j}-\phi_{P_0}}{a}b}{\Delta V} = \sum_{j=1}^{N}\rho_j\boldsymbol{U}_j\cdot\boldsymbol{n}_j\frac{\phi_{P_0}+\phi_{P_j}}{2}\frac{b}{\Delta V} - \sum_{j=1}^{N}\Gamma_j(\phi_{P_j}-\phi_{P_0})\frac{b}{a\Delta V}. \tag{17}$$

Assuming that x_j is the direction from P_0 to P_j, the Taylor expansions for ϕ_{P_j} and ϕ_{P_0} at the midpoint of side j of a control volume are as follows:

$$\phi_{P_0} = \phi_j - \frac{\partial\phi}{\partial x_j}\frac{a}{2} + \frac{1}{2}\frac{\partial^2\phi}{\partial x_j^2}\left(\frac{a}{2}\right)^2 - \frac{1}{6}\frac{\partial^3\phi}{\partial x_j^3}\left(\frac{a}{2}\right)^3 + o\left(\left(\frac{a}{2}\right)^4\right), \tag{18}$$

$$\phi_{P_j} = \phi_j + \frac{\partial\phi}{\partial x_j}\frac{a}{2} + \frac{1}{2}\frac{\partial^2\phi}{\partial x_j^2}\left(\frac{a}{2}\right)^2 + \frac{1}{6}\frac{\partial^3\phi}{\partial x_j^3}\left(\frac{a}{2}\right)^3 + o\left(\left(\frac{a}{2}\right)^4\right). \tag{19}$$

Substituting Eqs. (18) and (19) into Eq. (17), we obtain

$$\sum_{j=1}^{N}\rho_j U_j\cdot\boldsymbol{n}_j\phi_j\frac{b}{\Delta V} - \sum_{j=1}^{N}\Gamma_j\frac{\frac{\phi_{P_j}-\phi_{P_0}}{a}b}{\Delta V} = \sum_{j=1}^{N}\rho_j\boldsymbol{U}_j\cdot\boldsymbol{n}_j\phi_j\frac{b}{\Delta V} - \sum_{j=1}^{N}\Gamma_j\frac{\partial\phi}{\partial x_j}\frac{b}{\Delta V} + \underbrace{\sum_{j=1}^{N}\rho_j\boldsymbol{U}_j\cdot\boldsymbol{n}_j\phi_j\frac{a^2b}{8\Delta V}\frac{\partial^2\phi}{\partial x_j^2}}_{tranction1} + \underbrace{\sum_{j=1}^{N}\Gamma_j\frac{a^2b}{24\Delta V}\frac{\partial^3\phi}{\partial x_j^3}}_{tranction2}. \tag{20}$$

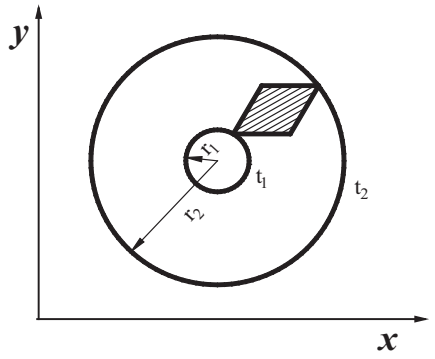

Fig. 3. Physical model and computational domain in Example A.

In Eq. (20), truncation1 and truncation2 are the truncation terms of convection term and diffusion term respectively. Here we define a_T and a_H as the length of the sides of the triangles and hexagons respectively. For the triangular control volume, we have $a = \sqrt{3}a_T/3$, $b = a_T$. Similarly, we have $a = \sqrt{3}a_H$, and $b = a_H$ for a hexagon control volume. For the same mesh, the length of the sides of triangles and hexagons satisfies $a_H = \frac{\sqrt{3}}{3}a_T$. Thus, the coefficient of truncation term of a cell-centered scheme is

$$\xi_c = \left(\frac{a^2 b}{\Delta V}\right)_{center} = \frac{\left(\frac{\sqrt{3}}{3}a_T\right)^2 \cdot a_T}{\frac{1}{2}\frac{\sqrt{3}}{2}a_T^2} = \frac{4}{3\sqrt{3}}a_T.$$

Similarly, for a cell-vertex scheme we have

$$\xi_v = \left(\frac{a^2 b}{\Delta V}\right)_{vertex} = \frac{(\sqrt{3}a_H)^2 \cdot a_H}{6 \times \frac{1}{2}\frac{\sqrt{3}}{2}a_H^2} = \frac{2}{\sqrt{3}}a_H = \frac{2}{3}a_T.$$

Above all, we have $\xi_c > \xi_v$, which means the truncation error of a cell-centered scheme is greater than that of a cell-vertex scheme for a triangular mesh.

4. Numerical examples

A heat conduction problem and a convection-diffusion problem are employed to verify the theoretical derivation. The computational domains are mapped by triangular grids and the governing equations are discretized by the cell-centered scheme and the cell-vertex scheme on the triangular mesh respectively. In this part, the accuracy and convergence rates of the two schemes are to be compared.

Table 1
Comparison of solution errors between the cell-centered and the cell-vertex scheme in Example A.

Number of triangular cells	Absolute error	
	Cell-centered scheme	Cell-vertex scheme
50	6.09×10^{-4}	1.14×10^{-6}
200	1.57×10^{-4}	4.09×10^{-7}
450	7.03×10^{-5}	7.18×10^{-7}
800	3.97×10^{-5}	3.34×10^{-7}
1250	2.53×10^{-5}	2.71×10^{-7}

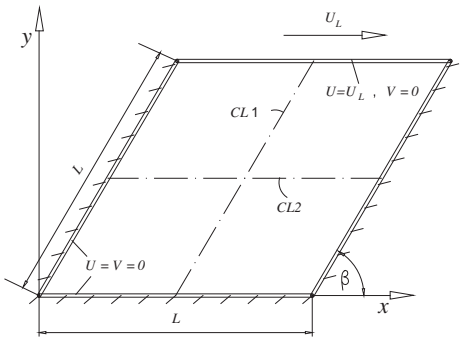

Fig. 5. Computational domain and boundary conditions for the lid-driven cavity flow problem in Example B.

4.1. Comparison of accuracy

4.1.1. Example A

For a cylinder of inside radius r_1 and outside radius r_2, with the boundary conditions $T = t_1$ at $r = r_1$ and $T = t_2$ at $r = r_2$ respectively (see Fig. 3), the temperature at any radius r can be calculated by the following equation (refer to [26]).

$$t = t_1 + \frac{t_2 - t_1}{\ln(r_2/r_1)}\ln(r/r_1) \tag{21}$$

The quality of the grids would affect the numerical accuracy. In order to compare the differences in accuracy and convergence rate between the cell-centered scheme and the cell-vertex scheme, the influence of the grids quality has to be eliminated. For a diamond domain shown in Fig. 3, it can be discretized by completely equilateral triangular cells, thus the control volumes for the cell-centered scheme and the cell-vertex scheme are all equilateral elements. For the cell-centered scheme, the variables are located at the centroids of the triangular cells, and the cells are control volumes, whereas for the cell-vertex scheme, the variables are located at the vertexes of triangular elements and the triangular cells are

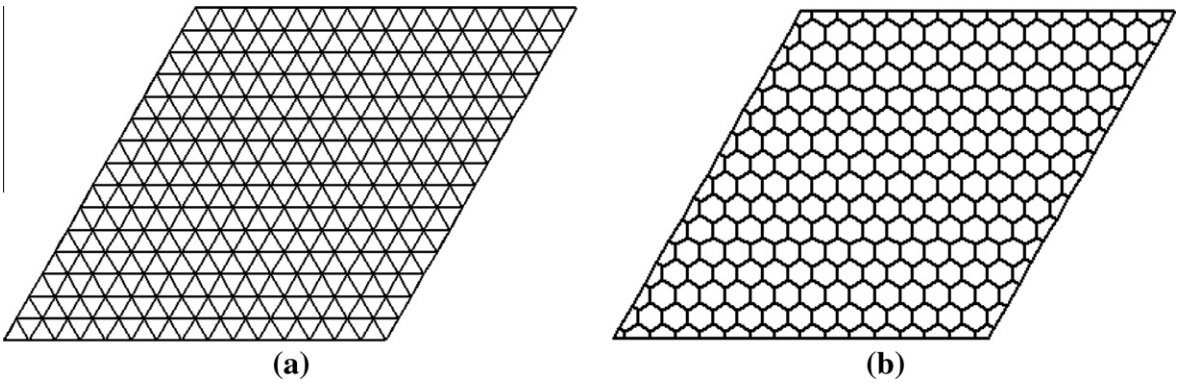

Fig. 4. Control volumes for (a) the cell-centered scheme and (b) the cell-vertex scheme in Example A.

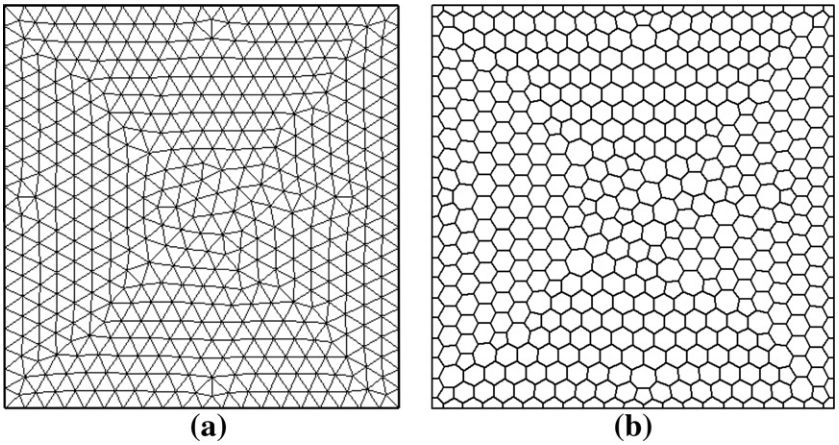

Fig. 6. Control volumes of (a) the cell-centered scheme and (b) the cell-vertex scheme in the square cavity flow problem in Example B.

not the control volumes. The control volumes of the cell-vertex scheme are hexagons as shown in Fig. 4.

In this example, five groups of triangular meshes consisting of different number of cells are generated for the computational domain. The numbers of triangular cells are 50, 200, 450, 800 and 1250 respectively. The solution errors of the cell-centered scheme and the cell-vertex scheme are listed in table 1. The 'Error' in the table is defined as mean absolute deviation between numerical solution and analytical solution. As can be seen from Table 1, the solution error of the cell-vertex scheme is smaller than that of the cell-centered scheme by two orders of magnitude.

4.1.2. Example B

The second example is a lid-driven cavity problem, and the computational domain and boundary conditions are illustrated in Fig. 5. In this part, a square cavity ($\beta = 90°$) and a skewed cavity ($\beta = 45°$) are discussed. The computational domains are mapped by triangular grids.

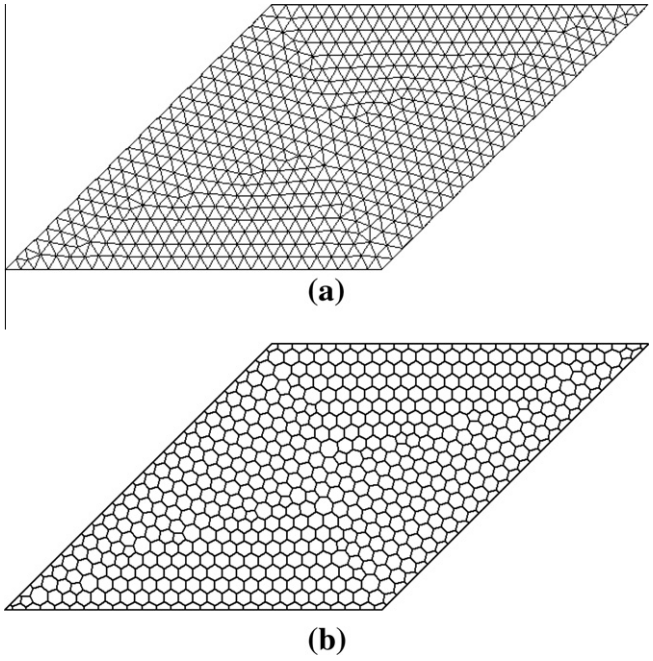

Fig. 7. Control volumes of (a) the cell-centered scheme and (b) the cell-vertex scheme in the skewed cavity flow problem in Example B.

The governing equation is discretized with a finite-volume method based on the cell-centered scheme and the cell-vertex scheme on triangular grids respectively. The control volumes for the cell-centered scheme are triangles shown in Fig. 6a, and for the cell-vertex scheme they are polygons shown in Fig. 6b. Figs. 6 and 7 reveal that the control volumes for the cell-centered scheme are grid cells (triangles) themselves and the numbers of neighboring elements of different control volumes are fixed, but for the cell-vertex scheme the control volumes are not the grid cells and the numbers of neighboring elements of different control volumes are varying.

The difference in accuracy between a cell-centered scheme and a cell-vertex scheme is mainly attributed to the difference in truncation error of these two schemes. If the mesh is dense enough, i.e. the grid independent solutions are obtained, the truncation errors of the two schemes should be identical and both schemes should lead to the same results. So the accuracy of the two schemes should be compared before the grid independent solutions are obtained.

In this example, Re is set at 1000. Based on the cell-centered scheme and the cell-vertex scheme, the governing equation is discretized on three groups of triangular meshes consisting of different number of cells.

Table 2
Comparison of average absolute errors between the cell-centered and the cell-vertex scheme in Example B.

Cell numbers	Average absolute error of U velocity component		Average absolute error of V velocity component	
	Cell-centered scheme	Cell-vertex scheme	Cell-centered scheme	Cell-vertex scheme
506	3.72×10^{-2}	2.00×10^{-2}	4.06×10^{-2}	1.91×10^{-2}
896	2.97×10^{-2}	1.24×10^{-2}	2.89×10^{-2}	1.24×10^{-2}
5628	5.78×10^{-3}	5.22×10^{-3}	4.91×10^{-3}	4.18×10^{-3}

Table 3
Comparison of average relative errors between the cell-centered and the cell-vertex scheme in Example B.

Cell numbers	Average relative error of U velocity component (%)		Average relative error of V velocity component (%)	
	Cell-centered scheme	Cell-vertex scheme	Cell-centered scheme	Cell-vertex scheme
506	30.47	13.94	35.42	15.09
896	22.64	8.47	23.16	9.22
5628	3.89	3.43	3.34	2.90

For the lid-driven square cavity problem, in order to compare the numerical errors of the cell-centered scheme and the cell-vertex scheme quantitatively, we calculated the U-velocity component and V-velocity component on a 160×160 mesh, and the results are set as the benchmark solution. The solution error can be obtained by comparing the numerical results with this benchmark solution. The average absolute errors and relative errors of the cell-centered scheme and the cell-vertex scheme for different grids are presented in Table 2 and Table 3 respectively. The average absolute error in Table 2 can be calculated by Eq. (22), and average relative error in Table 3 can be calculated by Eq. (23). As shown in Table 2 and Table 3, the average absolute error and relative error of the cell-vertex scheme are almost half of the cell-centered scheme for course mesh and the difference in error between these two schemes decreases with the increase of the number of cells.

$$Error_A = \frac{\sum_{i=1}^{N} |\phi_i - \hat{\phi}_i|}{N} \tag{22}$$

where ϕ_i is the numerical solution at node i, and $\hat{\phi}_i$ is the benchmark solution and N is the number of nodes.

$$Error_R = \frac{Error_A}{\bar{\phi}} \tag{23}$$

where

$$\bar{\phi} = \frac{\sum_{i=1}^{N} |\phi_i|}{N}.$$

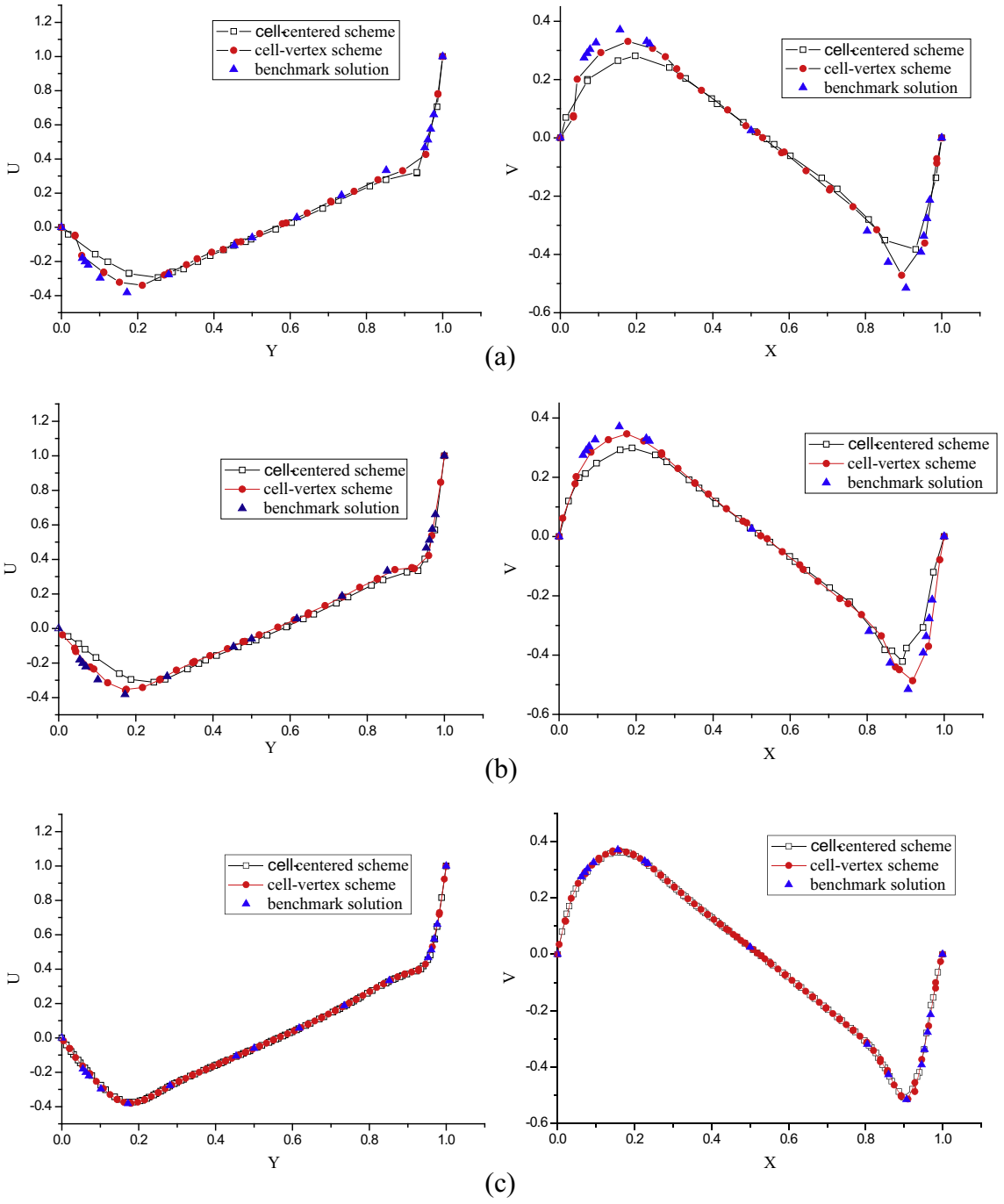

Fig. 8. Comparison of velocity components for the lid-driven square cavity flow problem in Example B on the grid consisting of (a) 506 cells, (b) 896 cells and (c) 5628 cells.

Besides, the velocity components at two centerlines CL1 and CL2 are compared with benchmark solution [27]. The U-velocity component at the centerline CL1 and V-velocity component at the horizontal centerline CL2 are depicted in Fig. 8 (square cavity) and Fig. 9 (skewed cavity) respectively. It is verified from the results shown in Figs. 8 and 9 that the solution of the cell-vertex scheme is much closer to the benchmark solution than that of the cell-centered scheme. In addition, as the number of cells increase, the numerical results are gradually reaching to the benchmark solution.

As disclosed in Figs. 8 and 9, before grid independent solution is obtained, the solutions of the cell-vertex scheme are closer to the benchmark solution, which indicates that for a triangular mesh, the cell-vertex scheme is more accurate than the cell-centered scheme, which makes it possible to use fewer grid cells to achieve the same accuracy and thus to save the computation time. This should be the first advantage of the cell-vertex scheme.

For the same case in Example B, if the convection term is discretized by SUD scheme, similar result can be obtained, i.e. the cell-vertex scheme is more accurate than the cell-centered scheme for the same triangular mesh. To be brief, only one group of results of a lid-driven skewed cavity (45°) problem is given in Fig. 10, which further demonstrates that the result of a cell-vertex scheme is more accurate than that of a cell-centered scheme.

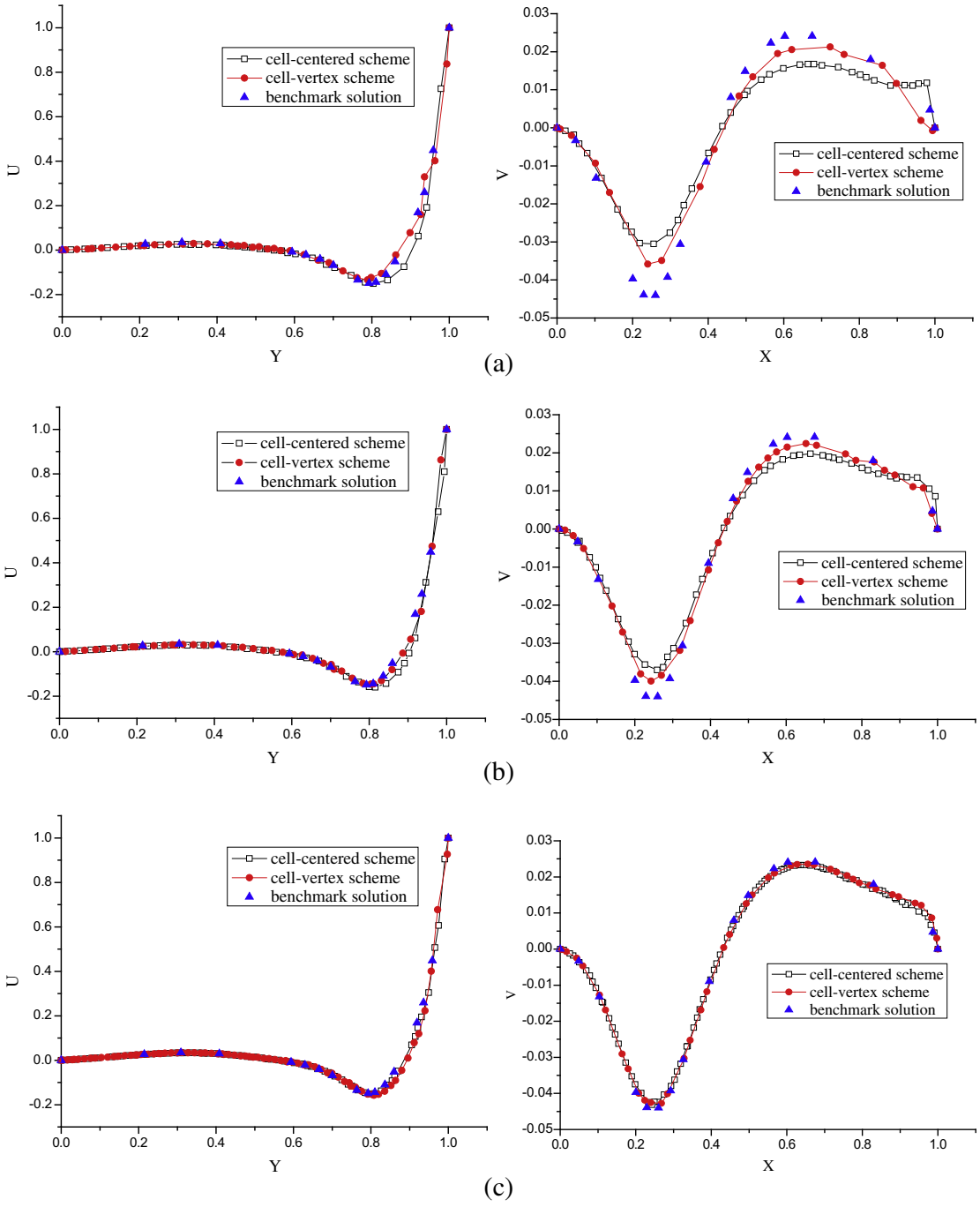

Fig. 9. Comparison of velocity components for the lid-driven skewed cavity (45°) flow problem in Example B on the grid consisting of (a) 1114 cells, (b) 2008 cells and (c) 5896 cells.

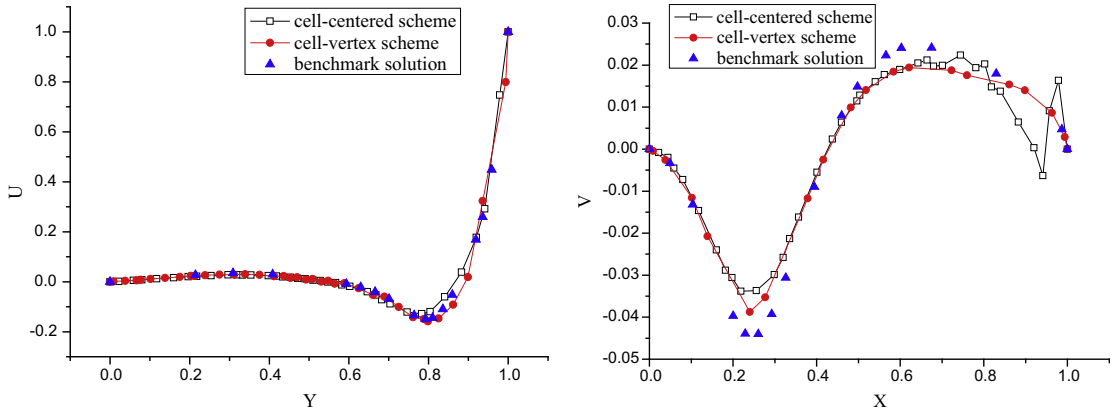

Fig. 10. Comparison of velocity components with the convection term discretized by SUD in Example B.

4.2. Comparison of convergence rates

The comparisons made above indicate that a cell-vertex scheme is more accurate than a cell-centered scheme for certain triangular grid. In this part, the difference in convergence rate between the cell-centered scheme and the cell-vertex scheme is to be compared.

It is known that the convergence rate is influenced by many factors, thus we must make sure they are compared under an identical circumstance including discretization of the governing equations, solution algorithm, iteration method for the algebraic equations, convergence criterion and mesh quality. As the grids employed in Example A are completely equilateral grids, the influence of grid quality would remain the same no mater a cell-centered scheme or a cell-vertex scheme is employed. In addition, the iteration scheme in this article is chosen to be a Gauss–Seidel scheme.

For the heat conduction problem in Example A, the convergence rates of the cell-centered scheme and the cell-vertex scheme are compared on five groups of grids consisting of different number of cells, and the comparisons disclose that the convergence rate of the cell-vertex scheme is much faster than that of the cell-centered scheme. For briefness, only one comparison is plotted in Fig. 11. Fig. 11a presents the variation of the norm of the residual as a function of performed iterations for the cell-centered scheme and the cell-vertex scheme, while Fig. 11b shows the variation of the norm of the residual as a function of computation time. It can be seen in Fig. 11 that the norm of residual of the cell-vertex scheme falls much more rapidly than that of the cell-centered scheme. When the same norms of residual are obtained, the computation time of the cell-centered scheme is twice of that of the cell-vertex scheme.

In Example A, the convergence rates of the cell-centered scheme and the cell-vertex scheme are compared on completely equilateral grids. However, the grids employed in the calculations could not always be equilateral. It is reported in the paper [25] that the convergence rate is not seriously affected by the orthogonality of the mesh if the crossing angle of the grid lines is greater than 45°. Therefore, we could borrow this conclusion to our case and assume that if the gird cells do not deviate from equilateral severely, the convergence rate of the cell-vertex scheme should always be faster. In order to validate this assumption, we compare the convergence rates for the lid-driven cavity problems in Example B.

The convergence rates of the cell-centered scheme and the cell-vertex scheme are compared for different grids consisting of different number of cells, and the results show that the convergence rate of the cell-vertex scheme is much faster than that of the cell-centered scheme. Briefly, only parts of the results are presented here as shown in Fig. 12 and Fig. 13. The residual in Figs. 12 and 13 is defined as the residual of the pressure correction equation for the SIMPLE method. Fig. 12 shows the comparison of convergence rates between the cell-centered scheme and the cell-vertex scheme for the lid-driven skewed cavity flow problem with a skew angle of 45°, and Fig. 13 shows the comparison of convergence

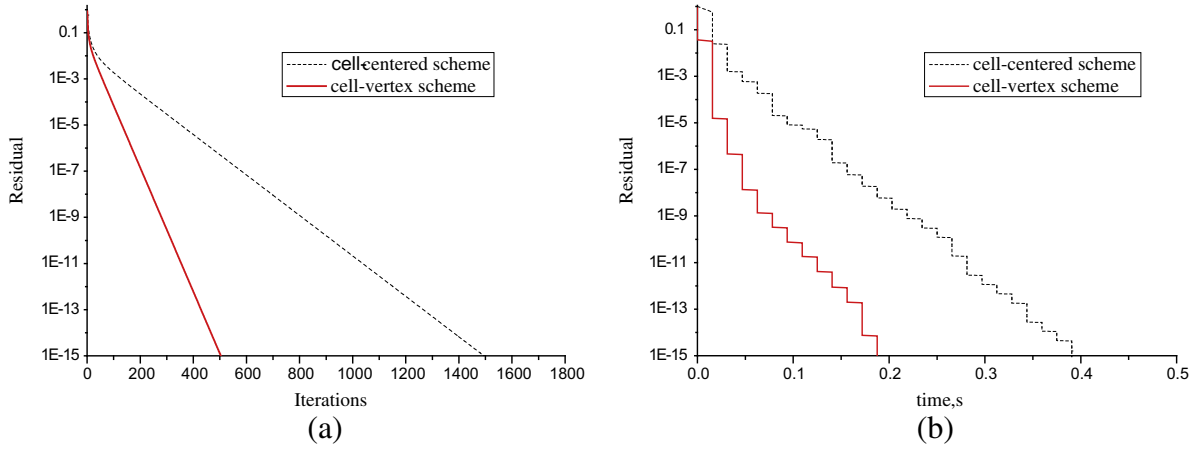

Fig. 11. Comparison of convergence rates for the heat conduction problem in Example A on the grid consisting of 1250 cells: (a) variation of residual as a function of iterations and (b) variation of residual as a function of time.

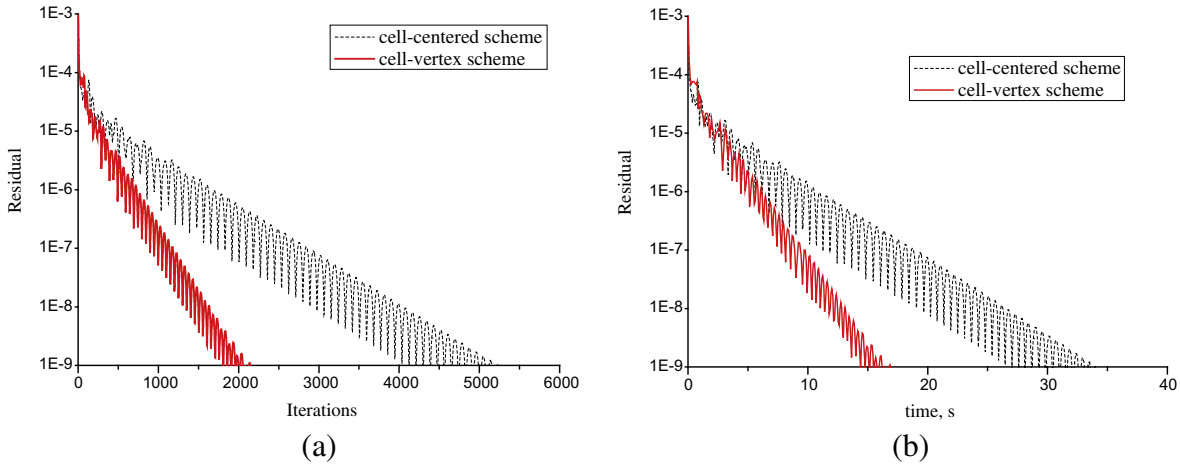

Fig. 12. Comparison of convergence rates for the lid-driven skewed cavity (45°) problem in Example B on a mesh consisting of 5896 cells.

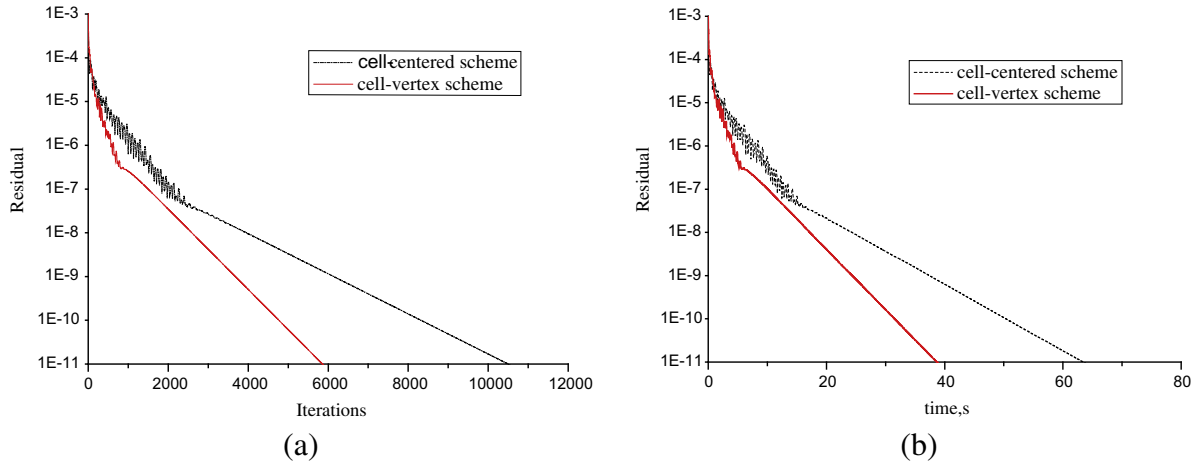

Fig. 13. Comparison of convergence rates for the lid-driven square cavity flow problem in Example B on the grid consisting of 5628 cells: (a) variation of residual as a function of iterations and (b) variation of residual as a function of time.

rates between the two schemes for a lid-driven square cavity flow problem. It can be seen in Figs. 12 and 13 that much less computation time is consumed by the cell-vertex scheme than by the cell-centered scheme. Fig. 13 presents that the computation time cost by the cell-vertex is 50% of that cost by the cell-centered scheme. Hence the second advantage of a cell-vertex scheme should be computation time-saving. In addition, it is also presented in Figs. 12 and 13 that the iterative oscillation of the cell-vertex scheme is smaller than the cell-centered scheme.

The reasons for the difference in convergence rates between the cell-centered scheme and the cell-vertex scheme can be analyzed from two aspects. First, the number of control volumes for the cell-vertex scheme is fewer than that for the cell-centered scheme, and fewer equations need to be solved, thus the convergence rate is faster. Second, it can be analyzed from a perspective of error vector attenuation. By Fourier analysis, error vector can be summed up by finite harmonics components, thus the converging process is a process of harmonics components attenuation. Among these harmonics components, there are long-wave components and short-wave components. It is known that, short-wave components decrease rapidly and the convergence rate mainly depend on long-wave components. We also know that long-wave components decrease effectively on course mesh, which is the basic idea of multigrid method. In one word, for the same grid, larger size of control

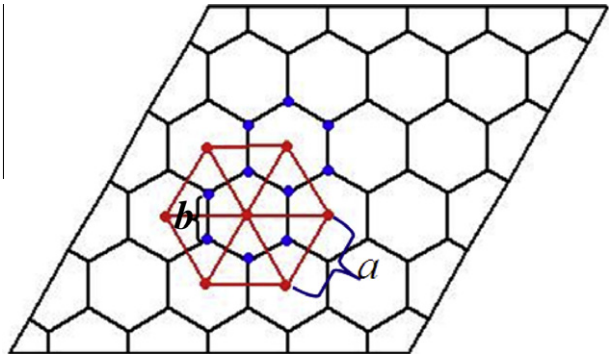

Fig. 14. The sizes of control volumes for a cell-centered scheme and a cell-vertex scheme.

volume is beneficial to convergence rate. Here the size of the control volume is defined as the distance between two adjacent nodes, i.e. for a cell-centered scheme, the control volumes are triangles shown in Fig. 14 and the size of control volume is b, while for a cell-vertex scheme, the control volumes are hexagons and the size of control volume is a. It can be calculated mathematically that $b = \sqrt{3}a/3$, that is the size of control volume for a cell-vertex

scheme *a* is larger than the size of control volume for a cell-centered scheme *b*. This should be why the convergence rate of a cell-vertex scheme is much faster than that of a cell-centered scheme.

5. Conclusions

The cell-vertex scheme for unstructured triangular meshes is not widely used in FVM due to the complexity of program implementation. However, there are some advantages in both numerical accuracy and convergence rate using this scheme. In this article, the numerical accuracy and convergence rate of the cell-vertex scheme and the cell-centered scheme are studied, and the results reveal that there are two advantages for the cell-vertex scheme: (1) on the same triangular mesh, the cell-vertex scheme is more accurate than the cell-centered scheme, in other words, fewer cells are required to achieve the same accuracy for a cell-vertex scheme; (2) on the same triangular mesh, the convergence of the cell-vertex scheme is much faster than that of the cell-centered scheme, thus much computation time can be saved.

Acknowledgements

The study is supported by National Key Projects of Fundamental R/D of China (973 Project: 2011CB610306) and National Science Foundation of China (Nos. 51176204 and 51134006).

References

[1] S.H. Lo, A new mesh generation scheme for arbitrary planar domains, Int. J. Numer. Methods Eng. 21 (8) (1985) 1403–1426.
[2] J. Peraire, M. Vahdati, K. Morgan, O.C. Zienkiewicz, Adaptive remeshing for compressible flow computations, J. Comput. Phys. 72 (2) (1987) 449–466.
[3] D.F. Watson, Computing the N-dimensional Delaunay tessellation with application to Voronoi polytopes, Comput. J. 24 (2) (1981) 167–172.
[4] A. Bowyer, Computing Dirichlet tessellations, Comput. J. 24 (2) (1981) 162–166.
[5] K. Shimada, D.C. Gossard, Bubble mesh: automated triangular meshing of non-manifold geometry by sphere packing, in: ACM Symposium on Solid Modeling and Applications, 1995, pp. 409–419.
[6] Lilong Wu, Bin Chen, Gaoling Zhou, An improved bubble packing method for unstructured grid generation with application to computational fluid dynamics, Numer. Heat Transfer, Part B: Fundam. 58 (5) (2010) 343–369.
[7] S. Sun, M.F. Wheeler, Anisotropic and dynamic mesh adaptation for discontinuous Galerkin methods applied to reactive transport, Comput. Methods Appl. Mech. Eng. 195 (25–28) (2006) 3382–3405.
[8] S.V. Patankar, Numerical Heat Transfer and Fluid Flow, Hemisphere, Washington, DC, 1980.
[9] R.C. Swanson, R. Radespiel, Cell centered and cell vertex multigrid schemes for the Navier–Stokes equations, AAA J. 29 (5) (1991) 697–703.
[10] M. Thomadakis, M. Leschziner, A pressure-correction method for the solution of incompressible viscous flows on unstructured grids, Int. J. Numer. Methods Fluids 22 (7) (1996) 581–601.
[11] J.Y. Murthy, S. Mathur, Periodic flow and heat transfer using unstructured meshes, Int. J. Numer. Methods Fluids 25 (6) (1997) 659–677.
[12] M. M. Athavale, Y. Jiang, A.J. Przekwas, Application of an unstructured grid solution methodology to turbomachinery flows, (1995) AIAA-95-0174.
[13] B. Yu, M.J. Lin, W.Q. Tao, Automatic generation of unstructured grids in 2D domain with Delaunay triangulation and its applications, Int. J. Heat Mass Transfer 35 (5) (1999) 361–370.
[14] S.R. Mathur, J.Y. Murthy, A pressure-based method for unstructured meshes, Numer. Heat Transfer, Part B 31 (2) (1997) 195–215.
[15] S. Muzaferijia, Adaptive finite volume method for flow predictions using unstructured meshes and multigrid approach, PhD thesis, University of London, London, 1994.
[16] M. Peric, R. Kessler, G. Scheuerer, Comparison of finite-volume numerical methods with staggered and colocated grids, Comput. Fluids 16 (4) (1988) 389–403.
[17] Bo Yu, Hiroyuki Ozoe, Wen-Quan Tao, A collocated finite volume method for incompressible flow on unstructured meshes, Prog. Comput. Fluid Dynam. 5 (3–5) (2005) 181–189.
[18] Minghai Xu, Wenquan Tao, Method on unstructured grid for incompressible flows, J. Xi'an Jiaotong Univ. 39 (1) (2005) 83–86.
[19] L. Davidson, A pressure correction method for unstructured meshes with arbitrary control volumes, Int. J. Numer. Methods Fluids 22 (4) (1996) 265–281.
[20] S. Rida, F. McKenty, F.L. Meng, M. Reggio, A staggered control volumes scheme for unstructured triangular grids, Int. J. Numer. Methods Fluids 25 (6) (1997) 697–717.
[21] C. Hsu, A curvilinear-coordinate method for momentum, heat and mass transfer or irregular geometry, PhD thesis, University of Minnesota, 1981.
[22] C. Prakash, A finite elements method predicting flow through ducts with arbitrary cross sections, PhD thesis, University of Minnesota, 1981.
[23] W.Q. Tao, Recent Advances in Numerical Heat Transfer, Beijing, 2000, pp. 194–197.
[24] J.F. Thompson, Z.U.A. Warsi, C.W. Mastin, Boundary fitted coordinate systems for numerical solution of partial differential equations—a review, Int. J. Comput. Phys. 47 (1982) 1–108.
[25] H.X. Hwang, A. Prosperetti, Effect of grid orthorgonality on the solution accuracy of the two-dimensional connection diffusion equation, Numer. Heat Transfer, Part B 26 (1994) 1–20.
[26] S.M. Yang, W.Q. Tao, Heat Transfer, Beijing, 1999, pp. 33.
[27] C.W. Oosterlee, P. Wesseling, A. Segal, Benchmark solutions for the incompressible Navier–Stokes equations in general coordinates on staggered grids, Int. J. Numer. Methods Fluids 17 (4) (1993) 301–321.